THE JOURNAL OF PHYSICAL CHEMISTRY C

Article

pubs.acs.org/JPCC

Understanding How Polymer Properties Control OPV Device Performance: Regioregularity, Swelling, and Morphology Optimization Using Random Poly(3-butylthiophene-*co*-3-octylthiophene) Polymers

Amy S. Ferreira,[⊥,†] Jordan C. Aguirre,[⊥,†] Selvam Subramaniyan,[‡] Samson A. Jenekhe,[‡] Sarah H. Tolbert,*[,†,§,∥] and Benjamin J. Schwartz*[,†,∥]

[†]Department of Chemistry and Biochemistry, University of California, Los Angeles, Los Angeles, California 90095-1569, United States

[‡]Departments of Chemical Engineering and Chemistry, University of Washington, Seattle, Washington 98195-1750, United States

[§]Department of Materials Science and Engineering, University of California, Los Angeles, Los Angeles, California 90095, United States

[∥]California NanoSystems Institute, University of California, Los Angeles, Los Angeles, California 90095, United States

Supporting Information

ABSTRACT: The performance of polymer:fullerene bulk heterojunction (BHJ) photovoltaics is highly sensitive to the morphology of the polymer within the active layer. To tune this morphology, we constructed both blend-cast and sequentially processed BHJ devices from the fullerene derivative [6,6]-phenyl-C_{60}-butyric acid methyl ester (PCBM), in combination with a series of random poly(3-butylthiophene-*co*-3-octylthiophene)s with different fractions of each monomer, with the goal of controllably varying the average polymer side-chain length. What we found, however, was that the most important parameter for predicting device performance across this series of polymers was the regioregularity of the particular synthetic batch of polymer used, not the average side-chain length. Moreover, we found that regioregularity affected device performance in different ways depending on the processing route: lower regioregularity led to improved performance for sequentially processed devices, but was detrimental to the performance of blend-cast devices. We argue that the reason for this anticorrelation is that regioregularity is the single most important determinant of the relative crystalline of the polymer. The relative crystalline fraction, in turn, determines the ability of the polymer to swell in the presence of solvents. Polymer swelling is key to BHJ formation via sequential processing, but can lead to overly mixed systems using traditional blend-casting methods. As a result, we find that the best performing polymer for sequentially processed devices is the worst performer for blend-cast devices and vice versa, highlighting the importance of using both processing methods when exploring new materials for use in BHJ photovoltaics.

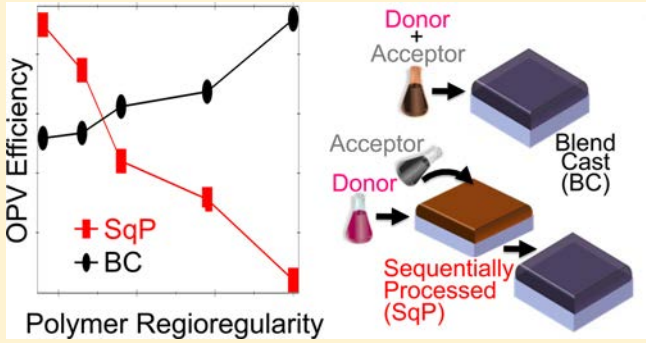

INTRODUCTION

Organic photovoltaics (OPVs) composed of semiconducting polymer donors have seen growing interest since efficiencies of over 10% were reached.[1,2] Most devices are composed of blended systems with conjugated polymers as the primary photoabsorbers and fullerene derivatives, such as [6,6]-phenyl-C_{60}-butyric acid methyl ester (PCBM), as the electron acceptors. For such systems, the photovoltaic efficiency is highly correlated with the nanometer-scale morphology of the blended components.[3] Due to low exciton diffusion lengths, the polymer and fullerene must be mixed on a 10−20 nm length scale to enable excitons to be split into free carriers at the donor/acceptor interface.[4] However, the two components also must have separate domains to prevent recombination[5] and to allow the free carriers to travel to their respective electrodes.[6,7] This type of morphology, known as a bulk-heterojunction (BHJ),[8] can be difficult to create by traditional blend-casting (BC) methods in which the polymer and fullerene are codissolved in solution and then cast into a film on a conductive substrate. This is because blend casting relies on spontaneous demixing of the two components during the drying process, and often requires a cosolvent or solvent additive.[9−11] Additional processing can also be performed after film formation by blend casting, including thermal anneal-

Received: March 31, 2016
Revised: August 26, 2016
Published: August 29, 2016

DOI: 10.1021/acs.jpcc.6b03300
J. Phys. Chem. C 2016, 120, 22115−22125

ing[12−14] and/or exposure to solvent atmosphere[15,16] to further demix the two phases. The final blend-cast film morphology is highly sensitive to these processing conditions and often requires an Edisonian, trial-and-error approach to optimize the extent of phase separation.[17]

An alternate approach to blend casting is sequential processing (SqP), in which a pure polymer film is first cast and dried, and then the fullerene layer is deposited on top of the polymer film in a second step.[18−26] In SqP, the fullerenes incorporate into the amorphous regions of the polymer film because the fullerene-casting solvent swells the underlying polymer film,[21,26−32] creating a BHJ morphology that can be similar to that formed through blend casting. Fullerene diffusion into the film can be further facilitated through thermal- or solvent-annealing postdeposition processes.[8,24,26,30,31] The SqP route tends to preserve the degree of crystallinity and other structural aspects of the initially deposited pure polymer film in the final BHJ morphology that is created, enabling fairly precise control over the BHJ architecture.[32−35]

Although SqP is generally a more controllable processing method, the morphology created in both blend casting and SqP is highly sensitive to the propensity of the polymer to crystallize.[24] Many groups have looked at controlling the relative crystalline fraction of the polymer by tuning either the polymer side chains or the polymer molecular weight, both of which can alter the resulting BHJ architecture.[36−38] We have previously shown that for poly(3-hexylthiophene) (P3HT), the degree of crystallinity has the opposite effect on the efficiency of devices fabricated by blend casting and SqP, with increased relative crystalline fractions improving the efficiency of blend-cast devices but decreasing the efficiency of sequentially processed devices.[24]

In this work, our initial goal was to further explore the extent to which the relative polymer crystallinity and paracrystallinity control the performance of OPV devices fabricated using different processing methods. To controllably tune polymer properties, we took advantage of a series of random copolymers, poly(3-butylthiophene-*co*-3-octylthiophene)s (RBO)s,[39] in which the percentage of 3-butyl versus 3-octyl side chains could be varied over a large range (Figure 1a). We note that random copolymers have been explored previously as a means to tune side-chain composition[40,41] or to incorporate heavier selenium atoms as a means to tune the polymer's energy levels.[42,43] Our plan was to explore the differences between blend casting and SqP by examining versions of the well-studied P3HT system with a continuously tunable average side chain length (Figure 1b). In this way, we planned to tune the relative crystalline fraction and thus the BHJ morphology without any changes in the system energetics.

What we found, however, was that BHJ morphology and device performance were not dominantly determined by the polymer side-chain composition, as we had expected, but instead were primarily correlated with the regioregularity of each batch of polymer. The regioregularity resulted from the synthetic details of each batch of polymer samples and varied nonmonotonically across the range of samples. We note that other groups have noted a relation between conjugated polymer regioregularity and the behavior of polymer/fullerene OPVs,[44−50] so in this work our aim became to precisely determine the correlation between regioregularity, relative crystalline fraction, and photovoltaic device performance. We find that the overall device performance and regioregularity

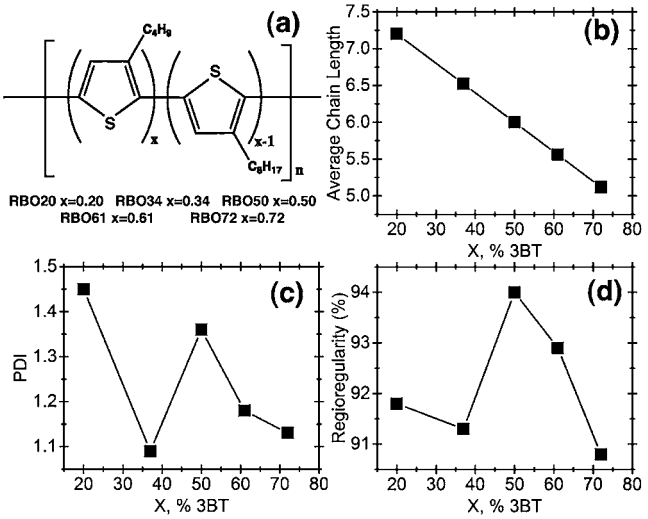

Figure 1. Characteristics of RBO_X used in this study: (a) chemical structure, (b) average chain length, (c) polydispersity index (PDI), (d) regioregularity.

were oppositely correlated with efficiency when optimizing OPV devices fabricated by SqP and blend casting, as summarized in the TOC graphic. We argue that this extraordinary sensitivity to regioregularity arises because regioregularity is the strongest predictor of the relative polymer crystalline fraction and in turn, polymer swelling. Swelling is an essential component in the formation of the BHJ morphology, particularly for fabrication via SqP.[31] Overall, we show that the steps taken to optimize BHJ formation with one type of processing result in highly nonideal morphologies for the other, so that both types of processing conditions must be explored to find the globally optimum device architecture for any given set of materials.

EXPERIMENTAL SECTION

We refer to the individual RBO polymers we used in this work as RBO_x, where x is the percent of butyl-thiophene monomers in the copolymer chain. We synthesized five random poly(3-butylthiophene-co-3-octylthiophene)[39] co-polymers with different percentages of butyl side changes: 20% (RBO_{20}), 34% (RBO_{34}); 50% (RBO_{50}); 61% (RBO_{61}); and 72% (RBO_{72}). We measured the regioregularities of these five co-polymers through ^{1}H NMR to be 91.8%, 91.3%, 94.0%, 92.9% and 90.8%, respectively. The number-average molecular weight and polydispersity index (PDI, also known as dispersity, Đ) for each RBO_x can be found in Table S1 of the Supporting Information (SI).

We fabricated the active photovoltaic device layers in this work using two basic processing conditions: "slow-dried", in which the OPV film spin-coating is halted while the film is still wet,[39] and "fast-dried", in which the active layer is spun until dry. All devices were fabricated on ITO substrates that were sequentially sonicated in baths of detergent, water, acetone, and isopropyl alcohol followed by UV ozone treatment for 10 min. Forty nanometers of poly(ethylenedioxythiophene):poly(styrenesulfonic acid) (PEDOT:PSS Clevios PVP AI 4083) was deposited onto ITO to form the hole collection layer.

For the blend-casting procedure, a 1:0.8 wt/wt RBO_x:$PC_{71}BM$ (Solenne, used as received) solution was made at a concentration of 20 mg/mL polymer/1,2

DOI: 10.1021/acs.jpcc.6b03300
J. Phys. Chem. C 2016, 120, 22115−22125

dichlorobenzene. This solution was deposited onto a PEDOT:PSS-coated substrate to produce films with a thickness of 115 ± 5 nm. Slow-dried films were allowed to fully dry in a N_2 atmosphere, then thermally annealed at 110 °C for 5 min. The fast-dried films were thermally annealed at 150 °C for 10 min. We held the fullerene ratio constant in this work to focus on the effects of side-chain length and regioregularity, but we note that polymers with lower regioregularity are able to accommodate a higher degree of fullerene loading, as we have discussed in previous work.[24]

Sequentially processed films were fabricated by depositing solutions of the pure RBO_x polymers onto PEDOT:PSS-coated substrates at 1000 rpm for 60 s (fast-dried) or 30 s (slow-dried) at a concentration of 20 mg/mL in 1,2 dichlorobenzene. $PC_{71}BM$ was deposited onto the fully dry polymer layer by spin coating at 4000 rpm for 10 s from a 10 mg/mL solution in dichloromethane. Both sequentially processed and blend-cast processed films were thermally annealed at 150 °C for 10 min (fast-dried) or 110 °C for 5 min (slow-dried). Ten nanometers of Ca and 70 nm of Al were thermally evaporated (Angstrom Engineering) as cathodes.

Samples for GIWAXS were fabricated similarly to the photovoltaic devices with the exceptions that Si was used as the substrate (with a native ∼2 nm thick oxide overcoated by 40 nm of PEDOT:PSS) instead of ITO on glass, and $PC_{61}BM$ (Nano-C) was substituted for $PC_{71}BM$. Although changing from the C_{60} to C_{70} version of the fullerene might change the polymer and/or fullerene crystallinities, the trends observed across the RBO_x series are expected to remain the same. The thicknesses of all films were found to be comparable using profilometry (Dektak). GIWAXS data was taken on three samples for each processing condition and corrected for fluctuations in beam intensity to ensure reproducibility. The polymer:fullerene ratio between blend-cast and sequentially processed films using a given RBO_x donor was matched using the redissolved film absorption spectroscopy method detailed by Hawks et al.[23]

Photovoltaic performance was measured in an Ar atmosphere using a Keithly 2400 source meter and AM-1.5-filtered light from a xenon arc lamp equipped with a liquid light guide (Oriel). The incident light intensity on tested samples was adjusted to be 100 mW/cm^2 using a calibrated Si diode. All photovoltaic efficiencies were verified by comparing the measured short-circuit current to the integrated external quantum efficiency (EQE), as detailed in the SI.

Grazing-incidence wide-angle X-ray scattering (GIWAXS) measurements were performed at the Stanford Synchrotron Radiation Lightsource (SSRL) on beamline 11-3 using a wavelength of 0.9742 Å. The diffraction patterns were collected on a 2-D image plate with the detector 400 mm from the sample center. The beam spot was approximately 150 μm wide, and a helium chamber was used to reduce air scatter and improve signal-to-noise. The WxDiff software package was used to radially integrate scattering data. This was accomplished by taking a fixed arc in chi of each diffractogram that includes both in-plane and out-of-plane scattering. The subsequent 1-D data was then corrected for the background silicon scattering. Since scattering peaks lose intensity with increasing scattering angle, a q^2 correction was performed to ensure that the (100) and (200) scattering intensities could be compared across the polymer series. We note, however, that the peak shifts across the different RBO_x polymers were small enough that the q^2 correction did not affect any of the results. The patterns shown in the main text are results average from three separate films. Each diffractogram was fit to a series of Gaussian curves. The increase in the full width at half-maximum (fwhm) across the overtones of the (100) scattering planes was used to determine the *g*-factor, which is correlated with the paracrystalline disorder.[50] The subsequent *g*-factors for each separate film were averaged together for the correlation calculations. The integrated GIWAXS peaks provide information about the relative polymer crystallinity across the series, and the *g*-factor allows us to better understand correlations between regioregularity and device performance with disorder in the polymer/fullerene films.

Polymer swelling was measured *in situ* using a PS-1000 Semilab ellipsometric porosimeter; experiments following the methods outlined by Huttner et al.[51] Pure polymer films were deposited onto silicon substrates with a native oxide layer using both the fast-dried and slow-dried methods described above. Ellipsometric measurements were taken at the approximate Brewster angle of silicon, 75°. The data were fit using the Semilab Spectroscopic Ellipsometry Analyzer (SEA) software, using a multilayer model for the silicon substrate and the native oxide layer. The Cauchy model was used for the thin polymer film to fit the $\tan(\Psi)$ and $\cos(\Delta)$ parameters directly measured by the ellipsometer, as described in more detail in the SI. No significant differences were found in the fitting parameters when anisotropy (i.e., birefringence) in the polymer films was included in the model, so for simplicity, the data presented here was fit assuming an isotropic (single n and k) polymer film.[52] To minimize contributions from the polymer absorption, we used the 800−1000 nm region for our fits. The (unswelled) film thicknesses measured by ellipsometry were confirmed by direct measurement with a Dektak profilometer. The swelling measurements used toluene vapor both because of its compatibility with the porosimeter instrument and because it is a good solvent for the RBO_X polymers that yields large volume changes during swelling. Vapor pressures were measured as relative pressure (p/p_{sat}), using the saturation pressure p_{sat} for toluene at room temperature of 29 Torr. The refractive indexes that we measured were validated using reported values.[19,53] Since the transparent region of the ellipsometry data was used for fitting, changes in the refractive index with swelling and solvent incorporation were fully taken into account. We note that we have shown in previous work that only the amorphous regions of P3HT films swell to any significant degree, so that our swelling measurements complement the GIWAXS data by providing additional information on noncrystalline regions of the BHJ films.

Although there are variations in the properties of each RBO_x polymer so that the behavior of photovoltaic devices fabricated from these materials cannot be perfectly predicted by any given polymer property, what is of greatest interest is to determine the degree of correlation between RBO_x properties and device performance. To determine correlations between different parameters, we used the Pearson product−moment correlation coefficient (r), given as[54]

$$r = \frac{\sum (x - \bar{x})(y - \bar{y})}{\sqrt{\sum (x - \bar{x})^2 \sum (y - \bar{y})^2}} \quad (1)$$

where x and y are the data sets to be linearly correlated. All correlation coefficients are given in Table 1. Although it is possible that the correlation could be nonlinear, we found that

DOI: 10.1021/acs.jpcc.6b03300
J. Phys. Chem. C 2016, 120, 22115−22125

Table 1. Summary of Pearson Product−Moment Correlation Coefficients between $RBO_x/PC_{71}BM$ Power Conversion Efficiency and RBO_x Polymer Properties

active layer	regioregularity	PDI	average side-chain length
slow dried SqP	−0.96	−0.65	−0.25
slow dried BC	0.95	0.35	−0.27
fast dried SqP	−0.94	−0.57	−0.28
fast dried BC	0.75	0.57	0.62

the use of the linear Pearson correlation coefficient worked well with our limited data set of only five distinct copolymers.

RESULTS AND DISCUSSION

We synthesized five RBO_x random copolymers with butyl side-chain percentages of 20%, 34%, 50%, 61%, and 72% following procedures published previously.[39] The PDI and regioregularity, which are both known to affect the polymer crystallinity and structure,[3,45,55−57] also were measured[39] and are summarized in Figure 1c,d, respectively, as well as Table S1. Our original goal was to focus on average side chain length, rather than regioregularity or polydispersity. Although we tried to synthesize the different RBO_x polymers in as similar a manner as possible, we were not able to precisely control the degree of regioregularity of each synthetic batch of polymer, creating a nonmonotonic trend between average side chain length and regioregularity. For this family of compounds, RBO_{50} has the highest regioregularity of the five RBO_x polymers studied. RBO_{20} and RBO_{72}, by contrast, even though they have drastically different monomer compositions, have regioregularities that are quite similar. These latter two materials thus provide a means to isolate which factor is more important for controlling the BHJ morphology and device performance: regioregularity or average side chain length.

A. Device Performance for the RBO_x Series with Different Processing Conditions. To begin our study, we fabricated both blend-cast and sequentially processed RBO_x:$PC_{71}BM$ BHJ devices using the various processing conditions summarized above. The average power conversion efficiency and full average $J-V$ curves for the best performing devices are plotted in Figure 2. The full average $J-V$ curves for the processing conditions not shown in Figure 2 and other performance characteristics are given in the SI. It has been shown previously that kinetics of film formation are improved in blend-cast devices when slow-drying is used to increase the ability of the polymer to reorganize and crystallize, rather than being locked into a more amorphous, mixed architecture.[58] Our results for blend-cast samples (red squares) fit with this expectation, with the slow-dried samples (panel c) outperforming the fast-dried samples (panel d). For both drying conditions, the blend-cast (BC) devices with the best efficiency were made using RBO_{50}, whereas RBO_{20} and RBO_{72}, which have identical regioregularity but very different side chains, produced devices with lower efficiencies. We calculated the correlation factor (eq 1) for the device efficiencies with various characteristics of the different RBO_x polymer batches, and the results are summarized in Table 1 with additional details given in the SI. Perhaps the most striking feature is that the overall efficiency trend for the blend-cast devices with both drying conditions reflects the trend in regioregularity plotted in Figure 1d: the correlation factors for both fast- and slow-dried blend-cast device efficiencies with polymer regioregularity are 0.75 and 0.95, respectively, suggesting that regioregularity is indeed

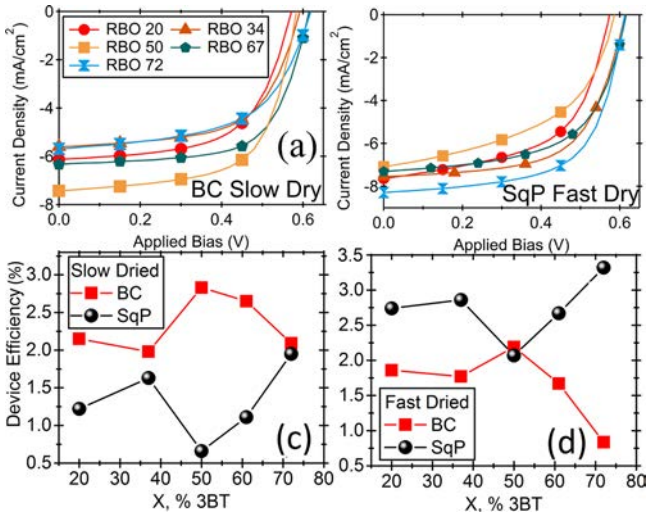

Figure 2. $J-V$ curves for slow-dried blend-cast (a) and fast-dried SqP films (b). The J-V curves for fast-dried blend-cast films and slow-dried SqP films are given in the SI. Photovoltaic device efficiency (%) for sequentially processed and blend-cast RBO_x/PCBM films fabricated with the slow-dried method (c) and fast-dried method (d).

an important factor in determining device efficiency. This is in agreement with previous work that shows that regioregularity in polythiophenes leads to an increase in interchain stacking that results in higher time-of-flight mobilities and dark-current densities indicating better charge extraction from the device.[44] The correlation between device efficiency and PDI also was calculated (Table 1), but the correlation factors were far lower: there is no apparent trend with x, the average side-chain composition.

The other striking feature of Figure 2 is that there is almost complete anticorrelation between blend-cast and sequentially processed devices (black circles, panels c and d) in terms of their efficiencies. The sequentially processed devices show an inverse effect of regioregularity, with a high anticorrelation factor (≤ -0.9; see Table 1); the RBO_{50} material gives the lowest device performance for SqP. Additionally, the trend in device performance with drying conditions is also reversed between blend casting and SqP, where fast-drying the initial polymer film in SqP improves device performance. The fact that the optimal polymer material and processing conditions give precisely opposite trends for SqP and blend casting indicates that the overall kinetics of BHJ formation in these two fabrication processes is quite different.

B. Structural Studies of RBO_x:PCBM BHJ Active Layers. To understand precisely what it is about the processing conditions that correlates or anticorrelates with device performance for blend casting and sequential processing, respectively, we performed grazing incidence wide-angle X-ray scattering (GIWAXS) on all of the BHJ active layers to see if polymer crystallinity is at the root of these correlations. Crystalline regions are known to have a significant effect on device performance as they help create the energy cascade that leads to charge separation and facilitate charge transport. Crystalline regions are also the key to creating the BHJ morphology via either SqP or blend casting because of the low solubility of fullerene in crystalline polymer. To simplify the results for the sequentially processed active layers, we examined the structure of pure polymer films. This is because we have shown previously for P3HT that PCBM intercalates primarily

DOI: 10.1021/acs.jpcc.6b03300
J. Phys. Chem. C 2016, 120, 22115−22125

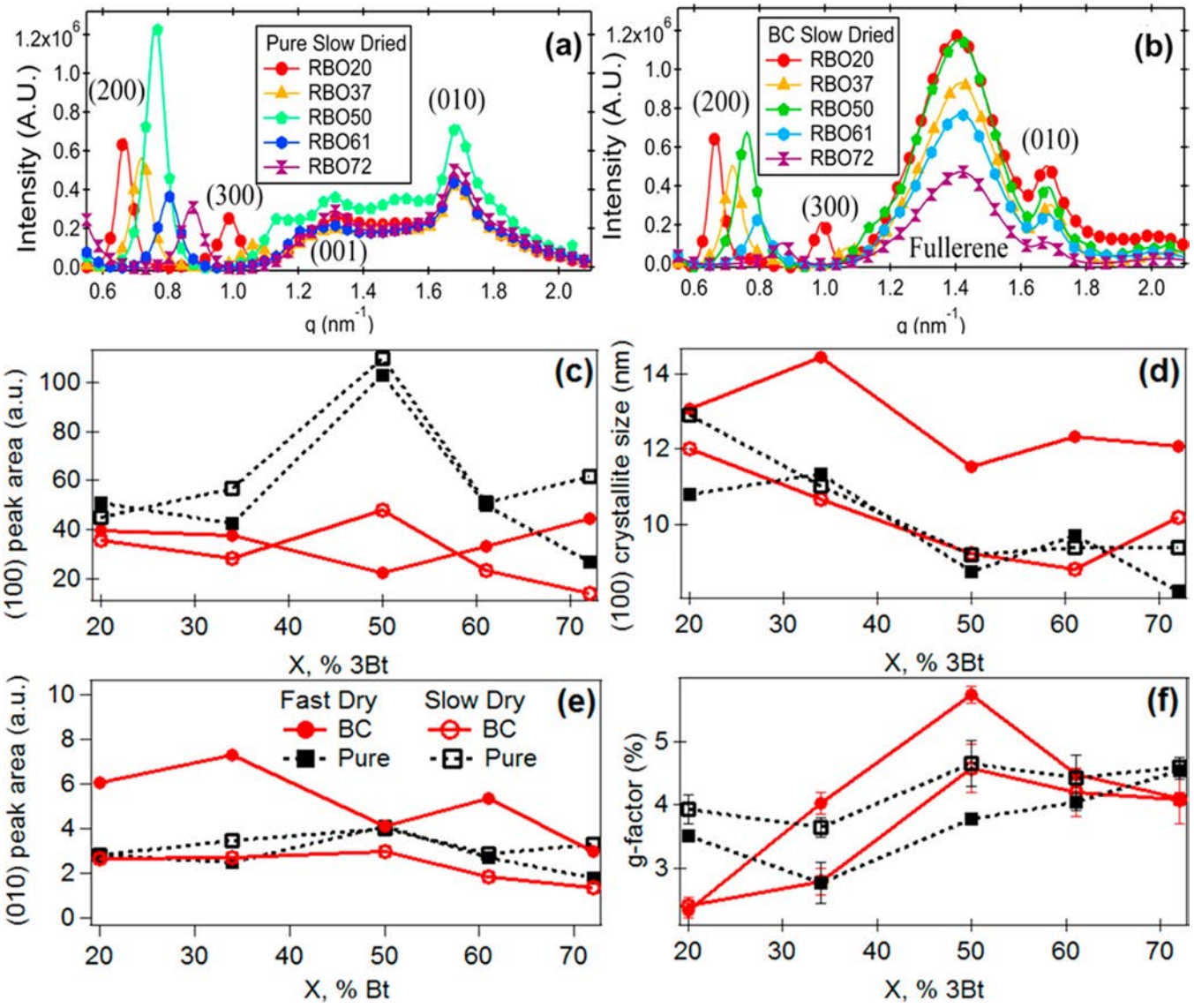

Figure 3. Integrated GIWAXS diffractograms for fast-dried pure polymer (a) and slow-dried blend-cast films (b). Diffractograms for fast dried films can be found in the SI. Gaussian fits to GIWAXS lamellar (100) peak area (c), (100) crystallite size (d), (010) crystallite size (e), and paracrystalline disorder (with one-sigma error bars) (f) for pure RBO$_x$ films (black curves, symbols) and RBO$_x$/PCBM BHJs (red curves, symbols). Integrated GIWAXS diffractograms for slow-dried pure polymer and fast-dried blend-cast films are given in the SI.

into the amorphous polymer regions during SqP, so that there is little change in X-ray-measurable polymer structure following sequential fullerene deposition.[23,24] The PCBM diffraction, however, overlaps the polymer diffraction and dramatically complicates analysis of the scattering data, as seen by the large peak at 1.4 nm^{-1} in Figure 3(b). For blend-cast samples, data from both pure polymer films and blend-cast active layers were considered because the blended films can show very different crystalline properties than the pure polymer films.

Since we have previously seen that polymer crystallinity plays an important role in both blend casting and sequential processing, we began by looking at the relative fraction of polymer crystallinity in both the lamellar (100) and $\pi-\pi$ stacking (010) directions. To do this, we radially integrated our 2-D GIWAXS diffractograms to obtain 1-D data, as shown in Figure 3 for fast-dried pure RBO$_x$ films (panel a) and slow-dried blend-cast films (panel b); integrated diffractograms for the processing conditions not shown in Figure 3 can be found in the SI. The resulting 1-D data was fit to a series of Gaussians, where the peak area corresponds to the relative crystalline fraction across the series and the peak width correlates to a Scherrer crystallite size or, more precisely, a domain correlation length.[50,59,60] The degree of paracrystalline disorder (*g*-factor) was also calculated from the spread of the full width at half-maximum (fwhm) of the lamellar peak, measured over multiple lattice overtones.[50] Since this analysis relies on multiple diffraction overtones, *g*-factors could not be calculated for the polymer (010) or fullerene peaks.

The results for pure RBO$_x$ polymer films (black) and blend-cast films with PCBM (red) are shown in Figure 3c–f. From the data in Figure 3, we can readily see that the relative polymer crystalline fraction and crystallite size do not follow a monotonic trend with side-chain length, as we would have expected based on the standard model of increased disorder associated with smaller side chains.[36,37] This same trend in relative crystalline fraction also was observed in DSC measurements on pure RBO$_x$ polymer films.[39] This provides strong evidence that the polymer crystalline properties, and in

DOI: 10.1021/acs.jpcc.6b03300
J. Phys. Chem. C 2016, 120, 22115–22125

Table 2. Summary of Pearson Product−Moment Correlation Coefficients between Different GIWAXS Parameters of the RBO_x Films Used in This Study and the RBO_x Regioregularity (RR), Polydispersity Index (PDI), and Side-Chain Length[a]

correlation parameter	(100) peak area			(100) crystallite size			g-factor		
active layer	RR	PDI	side-chain	RR	PDI	side-chain	RR	PDI	side-chain
slow dried SqP	0.68	0.22	0.24	−0.37	0.47	−0.89	0.45	0.08	0.79
slow dried BC	0.74	0.72	−0.53	−0.59	0.34	−0.73	0.55	−0.17	0.84
fast dried SqP	0.91	0.57	−0.14	−0.23	0.04	−0.83	0.03	−0.01	0.79
fast dried BC	−0.96	−0.36	−0.02	−0.55	−0.33	−0.61	0.63	−0.25	0.58

[a]All SqP correlations are using pure polymer diffraction, not BHJs.

turn the BHJ morphology, are not a very strong function of the side-chain length but are instead mostly dependent on other factors.

Looking at the trends in relative crystalline fraction for the pure polymer films, we see very little change in the (010) peak area across the RBO_x series (Figure 3e), but striking changes in the (100) peak area (Figure 3c). We thus use the (100) peak area as a rough measure of relative fraction of RBO_x crystallinity. By this measure, for sequentially processed films with both drying conditions and for slow-dried blend-cast films, RBO_{50} has the highest relative crystalline fraction. The general trend is that pure polymer relative crystalline fraction correlates well with polymer regioregularity, correlates somewhat with polymer PDI, and does not correlate at all with chain composition, as summarized in Table 2. To ensure the accuracy of our measured relative crystalline fractions, we also performed the same analysis using the (200) lamellar peaks and found the same trend, as shown in more detail in the SI. On the other hand, the extent of paracrystalline disorder, which is a measure of the long-range coherence of the crystalline packing,[36,61−63] correlates well with the average side-chain length, with the shortest side-chain length associated with the largest disorder, as expected. Since order in the backbone of the polymer is seen in the relative crystalline fraction, this correlation most likely reflects disorder within the side chains.

In contrast to the correlations found with pure polymer films, Table 2 shows that blend-cast RBO_x films show almost no correlation between polymer regioregularity and relative crystalline fraction. This is rather surprising given that it is generally accepted that both increasing side-chain length and increasing polymer regioregularity improves polymer $\pi-\pi$ overlap by promoting interchain ordering.[64,65] Clearly, there is not a simple relationship between the synthetic parameters of the pure polymer and the polymer's relative crystalline fraction in a blended system. Instead, a large variety of both polymer and fullerene characteristics play a role in the demixing that occurs during the drying (and thermal or solvent annealing) of blend-cast films, so that there is no easy way to predict the final BHJ morphology.[17]

To better assess how the relative fraction of polymer crystallinity is related to the BHJ morphology of blended films, we examined the correlation between device efficiency and different GIWAXS parameters. Table 3 shows the correlation of blend-cast and sequentially processed device efficiency with both the blend-cast GIWAXS parameters and the pure polymer GIWAXS parameters across the RBO_x polymer series. The sequentially processed device efficiencies strongly anticorrelate with the blend-cast device efficiencies, as expected based on our previous work showing that sequentially processed devices need more amorphous regions for fullerene intercalation, while blend-cast devices need a higher relative crystalline fraction to drive phase separation.[37] However, the blend-cast device

Table 3. Summary of Pearson Product−Moment Correlation Coefficients between $RBO_x/PC_{71}BM$ Device Power Conversion Efficiency and Different GIWAXS Parameters Used in This Study

active layer	(100) area	(010) area	(100) crystallite size	(010) crystallite size	g-factor
slow dried SqP	−0.57[a]	−0.35[a]	0.19[a]	−0.92[a]	−0.29[a]
slow dried BC	0.53[a]	0.21	−0.75	0.36	0.74
fast dried SqP	−0.96[a]	0.54[a]	−0.01[a]	−0.98[a]	0.15[a]
fast dried BC	−0.80	0.50	0.06	−0.85	0.20

[a]Data compared to pure polymer films instead of BHJs.

efficiencies also correlate more strongly to the relative crystalline fraction of the pure polymer than to that of the blend-cast polymer/fullerene composite. This indicates that rather than studying the more complicated mixed systems using X-ray diffraction, the pure polymer morphology is a better predictor of the final BHJ morphology and device performance.

One surprising feature of Table 3 is the essentially complete lack of correlation between (100) crystallite size and device efficiency for either blend-cast or sequentially processed RBO_x devices. Since large crystallites would prevent proper mixing, we expected that there would be an anticorrelation between crystalline domain size and device efficiency, which indeed we see in the slow-dried blend-cast case. The degree of crystallinity is a combination of the crystallite size, the defect density within those crystallites, and the relative number of crystallites. Thus, the lack of correlation of device performance with crystallite size for the other three fabrication conditions either indicates that as long as crystallites are below a certain size, reasonable performance is observed, or more likely, that defects within a crystallite do not significantly affect performance, and so a broad range of apparent domain sizes can correlate with similar physical crystallite sizes and thus similar device performance.

In addition, although there is a correlation between paracrystalline disorder and side-chain length, the paracrystallinity does not correlate with device efficiency. This suggests that disorder in the side-chains (rather than the semiconducting polymer backbone) does not play a significant role for the performance of devices fabricated by either SqP or blend-casting. We show in the SI that there is a strong correlation between the shape of the UV−visible absorption spectrum and device performance, as the absorption spectrum accurately reflects the type of order that is important for charge transport through the BHJ device.[67] We also show in the SI the correlation of relative fraction crystallinity with other device performance figures of merit, including the short-circuit current, open-circuit voltage, and fill factor. We find that the

DOI: 10.1021/acs.jpcc.6b03300
J. Phys. Chem. C 2016, 120, 22115−22125

relative fraction of crystallinity does not affect the open-circuit voltage of the devices, a result consistent with drift−diffusion simulations that have shown that V_{OC} is relatively impervious to disorder and local environment.[68] Instead, the correlation between relative crystalline fraction and device efficiency comes about because of correlation with both the short-circuit current and fill factor.

C. Swelling Studies of Pure RBO$_x$ Films. Even though the average side-chain length varies considerably across the RBO$_x$ series, why are the two most important factors that correlate with device efficiency the polymer regioregularity and the relative crystalline fraction in the pure film? We believe that answer is linked with how polymers of different regioregularity swell while being processing into BHJs. We have previously shown that polymer swelling is essential for producing high-efficiency photovoltaic devices fabricated through SqP, where the amorphous domains of the polymer are preferentially swollen.[31] We also believe that swelling plays an important role in the demixing of the polymer and fullerene during blend-casting, as discussed further below.

To understand how differences in regioregularity and relative crystalline fraction of the RBO$_x$ polymers are related to swelling, we measured the extent of swelling in both slow-dried and fast-dried RBO$_x$ films using spectroscopic ellipsometric porosimetry.[51,69−74] For these studies, we induced swelling by exposing the polymer films to controlled amounts of toluene vapor, which is a good solvent for all of the polymers in this series. Figure 4a,b shows the resulting swelling profiles that occurred for each RBO$_x$ using fast-drying and slow-drying. The maximum swelling of each film occurred at the saturation vapor pressure of toluene, 29 Torr. Figure 4c shows the maximum swelling of both fast-dried and slow-dried films of the pure polymers across the RBO$_x$ series, and Table 4 explores the correlations of swelling with various synthetic, structural, and device parameters. The swelling of both fast-dried and slow-dried RBO$_x$ films are anticorrelated to regioregularity, with the most regioregular polymers showing the lowest ability to swell. This result is expected, since highly regioregular polymers should have a higher fraction relative crystallinity, leaving fewer amorphous regions to uptake solvent.[28,31,58,59,66,75−77] We also see an anticorrelation between swelling and PDI, which we believe simply reflects the fact that, for this batch of samples, the more regioregular polymers also tended to have higher PDIs. We find little correlation between the average side-chain length and the amount of swelling in the RBO$_x$ films. If we expect swelling to be a major factor in controlling morphology and thus BHJ device performance, this again indicates that side-chain length is not an important factor in determining that morphology.

For the sequentially processed devices, we observe a strong correlation between swelling and device efficiency for both the slow-dried and fast-dried polymer samples. This fits well with our previous work showing that swelling is the dominant factor that controls fullerene intercalation, BHJ morphology, and thus the performance of sequentially processed devices.[31] Unexpectedly, we also see a modest anticorrelation between blend-cast device efficiency and pure polymer swelling in both the fast-dried (−0.69) and slow-dried (−0.41) cases. This provides strong evidence that swelling of a polymer film also plays a role in the kinetics of demixing that occurs during drying of blend-cast films. If the polymer is easily swollen, there is less driving force to cause phase separation of the polymer and the fullerene, creating a different BHJ morphology than would be obtained with a polymer that is difficult to swell. This correlation between demixing and swelling is part of what complicates the X-ray diffraction observed in blend-cast mixed

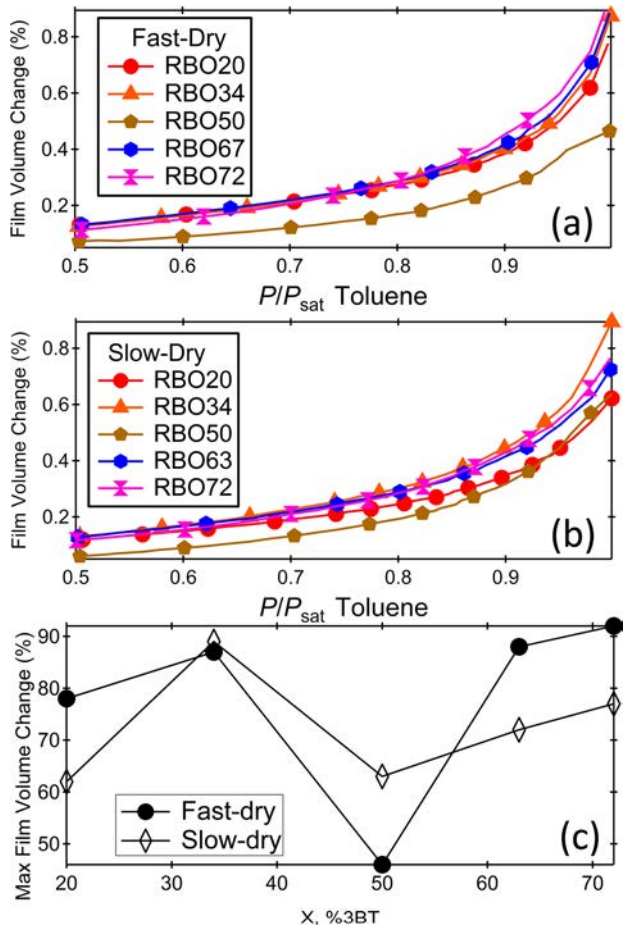

Figure 4. Ellipsometric porosimetry swelling profiles for fast-dried (a) and slow-dried (b) pure RBO$_x$ films. (c) The maximum volume change of swelled pure RBO$_x$ films taken at the saturation pressure of toluene (29 Torr).

Table 4. Summary of Pearson Product−Moment Correlation Coefficients between Pure RBO$_x$ Polymer Film Swelling at the Saturation Pressure of Toluene with Different Polymer Properties, Device Efficiency, and the Various GIWAXS Parameters Used in This Study

correlation to swelling	slow-dried	fast-dried
regioregularity	−0.60	−0.81
PDI	−0.91	−0.63
average side-chain length	−0.21	−0.20
SqP device efficiency	0.70	0.89
BC device efficiency	−0.41	−0.69
SqP paracrystallinity	−0.50	−0.01
SqP (100) peak area	−0.57	−0.47
SqP (100) crystallite size	−0.03	0.13
SqP (010) peak area	−0.37	0.26
SqP (010) crystallite size	−0.54	−0.84
BC paracrystallinity	−0.19	−0.54
BC (100) peak area	−0.56	0.47
BC (100) crystallite size	−0.02	0.48
BC (010) peak area	−0.26	0.19
BC (010) crystallite size	−0.20	0.45

DOI: 10.1021/acs.jpcc.6b03300
J. Phys. Chem. C 2016, 120, 22115−22125

polymer/fullerene films, explaining why the best correlations are to the fraction relative crystallinity of the pure polymer films. Thus, the crystallinity and swelling of pure polymers films, which are determined primarily by the polymer regioregularity, are much better predictors of the final blend-cast morphology than any parameter obtained through analysis of the BHJ film.

CONCLUSIONS

This work shows that it is the fundamental properties of conjugated polymer chains determined by their synthesis, such as the average chain regioregularity, that dominate BHJ morphologies produced by both SqP and blend-casting. Moreover, because SqP and blend-casting produce optimized BHJ morphologies from fundamentally different starting points, factors such as polymer regioregularity control device performance and morphology from these two processing routes in opposite ways. High polymer regioregularity is needed for blend-cast devices in order to drive phase separation between polymers and fullerenes that were molecularly mixed in the solution used to cast the film.[3344,45,74−78] When high polymer regioregularity is not present, other processing techniques that facilitate demixing must be used, such as thermal annealing[14,80] or the use of solvent additives[11,79,80] or solvent annealing.[72] In SqP, on the other hand, BHJ formation occurs only when the fullerene-casting solvent swells the underlying polymer film,[8,23,31,37] a process that is facilitated with polymer samples that have lower regioregularity and relative fraction crystallinity.

The initial goal of this work was to use polymer average side-chain length to direct morphology formation in both blend-cast and sequentially processed devices. What we found, however, is that the regioregularity of the polymer, which happened to vary from one batch to the next, is the primary polymer property associated with the overall BHJ morphology because of the way regioregularity impacts crystallinity and swelling. We also found that the relative fraction crystallinity of pure polymer films is a better predictor of device performance than any structural characteristic of the BHJ blends. We note that the polythiophene derivatives studied in this work, even those with lower regioregularity, tend to have higher relative crystalline fractions, whereas low bandgap, high-efficiency push−pull polymers tend to be much more amorphous. This suggests that regioregularity effects like those observed here could be even more important with low bandgap materials that have little fraction crystallinity and thus little driving force for demixing with fullerenes in blend-cast devices; control over swelling of those materials is likely to be even more important for BHJ formation. This also suggests that the generally more amorphous low-bandgap polymers should be more amenable to SqP than blend-casting, even though most of the work in the literature with these materials has focused on blend-casting. Thus, although the correlations in this paper do not necessarily prove causation, they do show that the regioregularity of a polymer batch is far more important in determining device properties than is typically considered in the literature, and that different processing methods can be chosen to take advantage of the various polymer properties correlated with regioregularity.

Finally, it is worth pointing out that the best sequentially processed device from this series, fabricated with RBO_{72}, outperforms the most efficient blend-cast device from this series, made with RBO_{50}. This shows the danger in focusing solely on the blend-cast fabrication technique to screen novel photovoltaic materials. Although there is only a small difference in device efficiency between the best blend-cast and SqP devices, these two processing methods favor different polymers within the RBO_x series. What is particularly striking is that the best material for one processing method is the other's worst performer. Therefore, knowledge gained by studying a materials series solely through the blend-casting method could be misleading, particularly since the effects of regioregularity, swelling, and crystallinity run in opposite directions for blend-casting and SqP. For the case of the RBO_x series, the highest-performing polymer RBO_{72} would have been entirely dismissed if only blend-cast films were studied. Clearly, it is necessary to consider multiple fabrication methods when screening new materials for photovoltaic performance.

ASSOCIATED CONTENT

Supporting Information

The Supporting Information is available free of charge on the ACS Publications website at DOI: 10.1021/acs.jpcc.6b03300.

(PDF)

AUTHOR INFORMATION

Corresponding Authors

*E-mail: tolbert@chem.ucla.edu; Tel: (310) 206-4767.

*E-mail: schwartz@chem.ucla.edu; Tel: (310) 206-4113.

Author Contributions

⊥These authors contributed equally to this work.

Notes

The authors declare no competing financial interest.

ACKNOWLEDGMENTS

This work was supported by the National Science Foundation (NSF) under grants CHE-1112569, CHE-1608957 and CBET-1510353. J.C.A. acknowledges previous support from the NSF IGERT: Materials Creation Training Program (MCTP), grant number DGE-0654431 and the California NanoSystems Institute. A.S.F. acknowledges support from The Clean Green IGERT (CGI), an energy-based NSF IGERT program (DGE-0903720). The X-ray diffraction studies presented in this manuscript were carried out at the Stanford Synchrotron Radiation Lightsource. Use of the Stanford Synchrotron Radiation Lightsource, SLAC National Accelerator Laboratory, is supported by the U.S. Department of Energy, Office of Science, Office of Basic Energy Sciences, under Contract DE-AC02-76SF00515. The authors wish to thank to Matthew Fontana and Taylor Aubry for fabricating the ellipsometry samples.

REFERENCES

(1) Green, M. A.; Emery, K.; Hishikawa, Y.; Warta, W.; Dunlop, E. D. Solar Cell Efficiency Tables (version 43). *Prog. Photovoltaics* **2015**, *23*, 1−9.

(2) He, Z.; Zhong, C.; Su, S.; Xu, M.; Wu, H.; Cao, Y. Enhanced Power-Conversion Efficiency in Polymer Solar Cells Using an Inverted Device Structure. *Nat. Photonics* **2012**, *6*, 593−597.

(3) Collins, B. A.; Tumbleston, J. R.; Ade, H. Miscibility, Crystallinity, and Phase Development in P3HT/PCBM Solar Cells: Toward an Enlightened Understanding of Device Morphology and Stability. *J. Phys. Chem. Lett.* **2011**, *2*, 3135−3145.

(4) Shaw, P. E.; Ruseckas, A.; Samuel, I. D. W. Exciton Diffusion Measurements in Poly(3-Hexylthiophene). *Adv. Mater.* **2008**, *20*, 3516−3520.

(5) Groves, C.; Marsh, R. A.; Greenham, N. C. Monte Carlo Modeling of Geminate Recombination in Polymer-Polymer Photovoltaic Devices. *J. Chem. Phys.* **2008**, *129*, 114903.
(6) Halls, J. J. M.; Walsh, C. A.; Greenham, N.; Marseglia, E. A.; Friend, R.; Moratti, S. C.; Holmes, A. Efficient Photodiodes from Interpenetrating Polymer Networks. *Nature* **1995**, *376*, 498−500.
(7) Shaheen, S. E.; Brabec, C. J.; Sariciftci, N. S.; Padinger, F.; Fromherz, T.; Hummelen, J. C. 2.5% Efficient Organic Plastic Solar Cells. *Appl. Phys. Lett.* **2001**, *78*, 841−843.
(8) Yu, G.; Gao, J.; Hummelen, J. C.; Wudl, F.; Heeger, A. J. Polymer Photovoltaic Cells: Enhanced Efficiencies via a Network of Internal Donor-Acceptor Heterojunctions. *Science (Washington, DC, U. S.)* **1995**, *270*, 1789−1791.
(9) Peet, J.; Soci, C.; Coffin, R. C.; Nguyen, T. Q.; Mikhailovsky, A.; Moses, D.; Bazan, G. C. Method for Increasing the Photoconductive Response in Conjugated Polymer/fullerene Composites. *Appl. Phys. Lett.* **2006**, *89*, 252105.
(10) Peet, J.; Kim, J. Y.; Coates, N. E.; Ma, W. L.; Moses, D.; Heeger, A. J.; Bazan, G. C. Efficiency Enhancement in Low-Bandgap Polymer Solar Cells by Processing with Alkane Dithiols. *Nat. Mater.* **2007**, *6*, 497−500.
(11) Lee, J. K.; Ma, W. L.; Brabec, C. J.; Yuen, J.; Moon, J. S.; Kim, J. Y.; Lee, K.; Bazan, G. C.; Heeger, A. J. Processing Additives for Improved Efficiency from Bulk Heterojunction Solar Cells. *J. Am. Chem. Soc.* **2008**, *130*, 3619−3623.
(12) Ma, W.; Yang, C.; Gong, X.; Lee, K.; Heeger, A. J. Thermally Stable, Efficient Polymer Solar Cells with Nanoscale Control of the Interpenetrating Network Morphology. *Adv. Funct. Mater.* **2005**, *15*, 1617−1622.
(13) Kim, K.; Liu, J.; Namboothiry, M. A. G.; Carroll, D. L. Roles of Donor and Acceptor Nanodomains in 6% Efficient Thermally Annealed Polymer Photovoltaics. *Appl. Phys. Lett.* **2007**, *90*, 163511.
(14) Verploegen, E.; Mondal, R.; Bettinger, C. J.; Sok, S.; Toney, M. F.; Bao, Z. Effects of Thermal Annealing Upon the Morphology of Polymer-Fullerene Blends. *Adv. Funct. Mater.* **2010**, *20*, 3519−3529.
(15) Zhao, Y.; Xie, Z.; Qu, Y.; Geng, Y.; Wang, L. Solvent-Vapor Treatment Induced Performance Enhancement of poly(3-Hexylthiophene):methanofullerene Bulk-Heterojunction Photovoltaic Cells. *Appl. Phys. Lett.* **2007**, *90*, 043504.
(16) Jo, J.; Na, S.-I.; Kim, S.-S.; Lee, T.-W.; Chung, Y.; Kang, S.-J.; Vak, D.; Kim, D.-Y. Three-Dimensional Bulk Heterojunction Morphology for Achieving High Internal Quantum Efficiency in Polymer Solar Cells. *Adv. Funct. Mater.* **2009**, *19*, 2398−2406.
(17) Heeger, A. J. 25th Anniversary Article: Bulk Heterojunction Solar Cells: Understanding the Mechanism of Operation. *Adv. Mater.* **2014**, *26*, 10−28.
(18) Ayzner, A. L.; Tassone, C. J.; Tolbert, S. H.; Schwartz, B. J. Reappraising the Need for Bulk Heterojunctions in Polymer/Fullerene Photovoltaics: The Role of Carrier Transport in All-Solution-Processed P3HT/PCBM Bilayer Solar Cells. *J. Phys. Chem. C* **2009**, *113*, 20050−20060.
(19) Gevaerts, V. S.; Koster, L. J. A.; Wienk, M. M.; Janssen, R. A. J. Discriminating between Bilayer and Bulk Heterojunction Polymer:-Fullerene Solar Cells Using the External Quantum Efficiency. *ACS Appl. Mater. Interfaces* **2011**, *3*, 3252−3255.
(20) Moon, J. S.; Takacs, C. J.; Sun, Y.; Heeger, A. J. Spontaneous Formation of Bulk Heterojunction Nanostructures: Multiple Routes to Equivalent Morphologies. *Nano Lett.* **2011**, *11*, 1036−1039.
(21) Treat, N. D.; Brady, M. A.; Smith, G.; Toney, M. F.; Kramer, E. J.; Hawker, C. J.; Chabinyc, M. L. Interdiffusion of PCBM and P3HT Reveals Miscibility in a Photovoltaically Active Blend. *Adv. Energy Mater.* **2011**, *1*, 82−89.
(22) Ayzner, A. L.; Doan, S. C.; Tremolet de Villers, B.; Schwartz, B. J. Ultrafast Studies of Exciton Migration and Polaron Formation in Sequentially Solution-Processed Conjugated Polymer/Fullerene Quasi-Bilayer Photovoltaics. *J. Phys. Chem. Lett.* **2012**, *3*, 2281−2287.
(23) Hawks, S. A.; Aguirre, J. C.; Schelhas, L. T.; Thompson, R. J.; Huber, R. C.; Ferreira, A. S.; Zhang, G.; Herzing, A. A.; Tolbert, S. H.; Schwartz, B. J. Comparing Matched Polymer:Fullerene Solar Cells Made by Solution-Sequential Processing and Traditional Blend Casting: Nanoscale Structure and Device Performance. *J. Phys. Chem. C* **2014**, *118*, 17413−17425.
(24) Zhang, G.; Huber, R.; Ferreira, A.; Boyd, S. D.; Luscombe, C. K.; Tolbert, S. H.; Schwartz, B. J. Crystallinity Effect in Sequentially Processed and Blend Cast Bulk-Heterojunction Polymer/Fullerene Photovoltaics. *J. Phys. Chem. C* **2014**, *118*, 18424−18435.
(25) Clark, J.; Silva, C.; Friend, R.; Spano, F. Role of Intermolecular Coupling in the Photophysics of Disordered Organic Semiconductors: Aggregate Emission in Regioregular Polythiophene. *Phys. Rev. Lett.* **2007**, *98*, 206406−206406−4.
(26) Van Franeker, J. J.; Kouijzer, S.; Lou, X.; Turbiez, M.; Wienk, M. M.; Janssen, R. A. J. Depositing Fullerenes in Swollen Polymer Layers via Sequential Processing of Organic Solar Cells. *Adv. Energy Mater.* **2015**, *5*, 1500464.
(27) Lee, K. H.; Schwenn, P. E.; Smith, A. R. G.; Cavaye, H.; Shaw, P. E.; James, M.; Krueger, K. B.; Gentle, I. R.; Meredith, P.; Burn, P. L. Morphology of All-Solution-Processed "Bilayer" Organic Solar Cells. *Adv. Mater.* **2011**, *23*, 766−770.
(28) Loiudice, A.; Rizzo, A.; Latini, G.; Nobile, C.; de Giorgi, M.; Gigli, G. Graded Vertical Phase Separation of Donor/acceptor Species for Polymer Solar Cells. *Sol. Energy Mater. Sol. Cells* **2012**, *100*, 147−152.
(29) Nardes, A. M.; Ayzner, A. L.; Hammond, S. R.; Ferguson, A. J.; Schwartz, B. J.; Kopidakis, N. Photoinduced Charge Carrier Generation and Decay in Sequentially Deposited Polymer/Fullerene Layers: Bulk Heterojunction vs Planar Interface. *J. Phys. Chem. C* **2012**, *116*, 7293−7305.
(30) Kim, D. H.; Mei, J.; Ayzner, A. L.; Schmidt, K.; Giri, G.; Appleton, A. L.; Toney, M. F.; Bao, Z. Sequentially Solution-Processed, Nanostructured Polymer Photovoltaics Using Selective Solvents. *Energy Environ. Sci.* **2014**, *7*, 1103−1109.
(31) Aguirre, J. C.; Hawks, S. A.; Ferreira, A.; Yee, P.; Subramaniyan, S.; Jenekhe, S. A.; Tolbert, S. H.; Schwartz, B. J. Sequential Processing for Organic Photovoltaics: Design Rules for Morphology Control by Tailored Semi-Orthogonal Solvent Blends. *Adv. Energy Mater.* **2015**, *5*, 1402020.
(32) Liu, Y.; Liu, F.; Wang, H. W.; Nordlund, D.; Sun, Z.; Ferdous, S.; Russell, T. P. Sequential Deposition: Optimization of Solvent Swelling for High-Performance Polymer Solar Cells. *ACS Appl. Mater. Interfaces* **2015**, *7*, 653−661.
(33) Collins, B. A.; Gann, E.; Guignard, L.; He, X.; McNeill, C. R.; Ade, H. Molecular Miscibility of Polymer−Fullerene Blends. *J. Phys. Chem. Lett.* **2010**, *1*, 3160−3166.
(34) Lee, K. H.; Zhang, Y.; Burn, P. L.; Gentle, I. R.; James, M.; Nelson, A.; Meredith, P. Correlation of Diffusion and Performance in Sequentially Processed P3HT/PCBM Heterojunction Films by Time-Resolved Neutron Reflectometry. *J. Mater. Chem. C* **2013**, *1*, 2593.
(35) Aguirre, J. C.; Ferreira, A.; Ding, H.; Jenekhe, S. A.; Kopidakis, N.; Asta, M.; Pilon, L.; Rubin, Y.; Tolbert, S. H.; Schwartz, B. J.; et al. Panoramic View of Electrochemical Pseudocapacitor and Organic Solar Cell Research in Molecularly Engineered Energy Materials (MEEM). *J. Phys. Chem. C* **2014**, *118*, 19505−19523.
(36) Babel, A.; Jenekhe, S. a. Alkyl Chain Length Dependence of the Field-Effect Carrier Mobility in Regioregular poly(3-Alkylthiophene)s. *Synth. Met.* **2005**, *148*, 169−173.
(37) Gadisa, A.; Oosterbaan, W. D.; Vandewal, K.; Bolsee, J. C.; Bertho, S.; D'Haen, J.; Lutsen, L.; Vanderzande, D.; Manca, J. V. Effect of Alkyl Side-Chain Length on Photovoltaic Properties of poly(3-alkylthiophene)/PCBM Bulk Heterojunctions. *Adv. Funct. Mater.* **2009**, *19*, 3300−3306.
(38) Shen, X.; Hu, W.; Russell, T. P. Measuring the Degree of Crystallinity in Semicrystalline Regioregular Poly(3-Hexylthiophene). *Macromolecules* **2016**, *49*, 4501.
(39) Wu, P. T.; Ren, G.; Jenekhe, S. A. Crystalline Random Conjugated Copolymers with Multiple Side Chains: Tunable Intermolecular Interaction and Enhanced Charge Transport and Photovoltaic Properties. *Macromolecules* **2010**, *43*, 3306−3313.

DOI: 10.1021/acs.jpcc.6b03300
J. Phys. Chem. C 2016, 120, 22115−22125

(40) Burkhart, B.; Khlyabich, P. P.; Thompson, B. C. Influence of the Ethylhexyl Side-Chain Content on the Open-Circuit Voltage in Rr-Poly(3-Hexylthiophene- Co −3-(2-Ethylhexyl)thiophene) Copolymers. *Macromolecules* **2012**, *45*, 3740−3748.
(41) Burkhart, B.; Khlyabich, P. P.; Cakir Canak, T.; LaJoie, T. W.; Thompson, B. C. Semi-Random" Multichromophoric Rr-P3HT Analogues for Solar Photon Harvesting. *Macromolecules* **2011**, *44*, 1242−1246.
(42) Gao, D.; Hollinger, J.; Jahnke, A. A.; Seferos, D. S. Influence of Selenophene−thiophene Phase Separation on Solar Cell Performance. *J. Mater. Chem. A* **2014**, *2*, 6058−6063.
(43) Yan, H.; Hollinger, J.; Bridges, C. R.; McKeown, G. R.; Al-Faouri, T.; Seferos, D. S. Doping Poly(3-Hexylthiophene) Nanowires with Selenophene Increases the Performance of Polymer-Nanowire Solar Cells. *Chem. Mater.* **2014**, *26*, 4605−4611.
(44) Kim, Y.; Cook, S.; Tuladhar, S. M.; Choulis, S. A.; Nelson, J.; Durrant, J. R.; Bradley, D. D. C.; Giles, M.; McCulloch, I.; Ha, C.-S.; et al. A Strong Regioregularity Effect in Self-Organizing Conjugated Polymer Films and High-Efficiency Polythiophene:fullerene Solar Cells. *Nat. Mater.* **2006**, *5*, 197−203.
(45) Mauer, R.; Kastler, M.; Laquai, F. The Impact of Polymer Regioregularity on Charge Transport and Efficiency of P3HT:PCBM Photovoltaic Devices. *Adv. Funct. Mater.* **2010**, *20*, 2085−2092.
(46) Woo, C. H.; Thompson, B. C.; Kim, B. J.; Toney, M. F.; Frechet, J. M. J. The Influence of poly(3-Hexylthiophene) Regioregularity on Fullerene-Composite Solar Cell Performance. *J. Am. Chem. Soc.* **2008**, *130*, 16324−16329.
(47) Sivula, K.; Luscombe, C. K.; Thompson, B. C.; Frechet, J. M. J. Enhancing the Thermal Stability of Polythiophene:fullerene Solar Cells by Decreasing Effective Polymer Regioregularity. *J. Am. Chem. Soc.* **2006**, *128*, 13988−13989.
(48) Sher, M.-J.; Bartelt, J. A.; Burke, T. M.; Salleo, A.; McGehee, M. D.; Lindenberg, A. M. Time- and Temperature-Independent Local Carrier Mobility and Effects of Regioregularity in Polymer-Fullerene Organic Semiconductors. *Adv. Electron. Mater.* **2016**, *2*, 1500351.
(49) Snyder, C. R.; Henry, J. S.; Delongchamp, D. M. Effect of Regioregularity on the Semicrystalline Structure of poly(3-Hexylthiophene). *Macromolecules* **2011**, *44*, 7088−7091.
(50) Lilliu, S.; Agostinelli, T.; Pires, E.; Hampton, M.; Nelson, J.; Macdonald, J. E. Dynamics of Crystallization and Disorder during Annealing of P3HT/PCBM Bulk Heterojunctions. *Macromolecules* **2011**, *44*, 2725−2734.
(51) Huttner, S.; Sommer, M.; Chiche, A.; Krausch, G.; Steiner, U.; Thelakkat, M. Controlled Solvent Vapour Annealing for Polymer Electronics. *Soft Matter* **2009**, *5*, 4206−4211.
(52) Ng, A.; Li, C. H.; Fung, M. K.; Djurišić, A. B.; Zapien, J. A.; Chan, W. K.; Cheung, K. Y.; Wong, W.-Y. Accurate Determination of the Index of Refraction of Polymer Blend Films by Spectroscopic Ellipsometry. *J. Phys. Chem. C* **2010**, *114*, 15094−15101.
(53) Hedley, G. J.; Ward, A. J.; Alekseev, A.; Howells, C. T.; Martins, E. R.; Serrano, L. A.; Cooke, G.; Ruseckas, A.; Samuel, I. D. W. Determining the Optimum Morphology in High-Performance Polymer-Fullerene Organic Photovoltaic Cells. *Nat. Commun.* **2013**, *4*, 2867.
(54) Pearson, K. Note on Regression and Inheritance in the Case of Two Parents. *Proc. R. Soc. London* **1895**, *58*, 240−242.
(55) Jiang, X. M.; Österbacka, R.; Korovyanko, O.; An, C. P.; Horovitz, B.; Janssen, R. A. J.; Vardeny, Z. V. Spectroscopic Studies of Photoexcitations in Regioregular and Regiorandom Polythiophene Films. *Adv. Funct. Mater.* **2002**, *12*, 587−597.
(56) Adachi, T.; Brazard, J.; Ono, R. J.; Hanson, B.; Traub, M. C.; Wu, Z.-Q.; Li, Z.; Bolinger, J. C.; Ganesan, V.; Bielawski, C. W.; et al. Regioregularity and Single Polythiophene Chain Conformation. *J. Phys. Chem. Lett.* **2011**, *2*, 1400−1404.
(57) Kohn, P.; Rong, Z.; Scherer, K. H.; Sepe, A.; Sommer, M.; Müller-Buschbaum, P.; Friend, R. H.; Steiner, U.; Hüttner, S. Crystallization-Induced 10-Nm Structure Formation in P3HT/PCBM Blends. *Macromolecules* **2013**, *46*, 4002−4013.
(58) Turner, S. T.; Pingel, P.; Steyrleuthner, R.; Crossland, E. J. W.; Ludwigs, S.; Neher, D. Quantitative Analysis of Bulk Heterojunction Films Using Linear Absorption Spectroscopy and Solar Cell Performance. *Adv. Funct. Mater.* **2011**, *21*, 4640−4652.
(59) Rogers, J. T.; Schmidt, K.; Toney, M. F.; Kramer, E. J.; Bazan, G. C. Structural Order in Bulk Heterojunction Films Prepared with Solvent Additives. *Adv. Mater.* **2011**, *23*, 2284−2288.
(60) Verploegen, E.; Miller, C. E.; Schmidt, K.; Bao, Z.; Toney, M. F. Manipulating the Morphology of P3HT−PCBM Bulk Heterojunction Blends with Solvent Vapor Annealing. *Chem. Mater.* **2012**, *24*, 3923−3931.
(61) Poelking, C.; Andrienko, D. Effect of Polymorphism, Regioregularity and Paracrystallinity on Charge Transport in Poly(3-Hexylthiophene) [P3HT] Nanofibers. *Macromolecules* **2013**, *46*, 8941−8956.
(62) Lilliu, S.; Agostinelli, T.; Verploegen, E.; Pires, E.; Hampton, M.; Al-Hashimi, M.; Heeney, M. J.; Toney, M. F.; Nelson, J.; Macdonald, J. E. Effects of Thermal Annealing upon the Nanomorphology of poly(3-Hexylselenophene)-PCBM Blends. *Macromol. Rapid Commun.* **2011**, *32*, 1454−1460.
(63) Noriega, R.; Rivnay, J.; Vandewal, K.; Koch, F. P. V; Stingelin, N.; Smith, P.; Toney, M. F.; Salleo, A. A General Relationship between Disorder, Aggregation and Charge Transport in Conjugated Polymers. *Nat. Mater.* **2013**, *12*, 1038.
(64) Sanyal, M.; Schmidt-Hansberg, B.; Klein, M. F. G.; Colsmann, A.; Munuera, C.; Vorobiev, A.; Lemmer, U.; Schabel, W.; Dosch, H.; Barrena, E. In Situ X-Ray Study of Drying-Temperature Influence on the Structural Evolution of Bulk-Heterojunction Polymer−Fullerene Solar Cells Processed by Doctor-Blading. *Adv. Energy Mater.* **2011**, *1*, 363−367.
(65) Shin, N.; Richter, L. J.; Herzing, A. A.; Kline, R. J.; DeLongchamp, D. M. Effect of Processing Additives on the Solidification of Blade-Coated Polymer/Fullerene Blend Films via In-Situ Structure Measurements. *Adv. Energy Mater.* **2013**, *3*, 938−948.
(66) Zhang, G.; Ferreira, A.; Huber, R.; Boyd, S. D.; Luscombe, C. K.; Tolbert, S. H.; Schwartz, B. J. Crystallinity Effect in Sequentially-Processed P3HT/PCBM Photovoltaics. Submitted for publication.
(67) Spano, F. C. Modeling Disorder in Polymer Aggregates: The Optical Spectroscopy of Regioregular poly(3-Hexylthiophene) Thin Films. *J. Chem. Phys.* **2005**, *122*, 234701−234715.
(68) Finck, B. Y.; Schwartz, B. J. Drift-Diffusion Modeling of the Effects of Structural Disorder and Carrier Mobility on the Performance of Organic Photovoltaic Devices. *Phys. Rev. Appl.* **2015**, *4*, 034006.
(69) Elbs, H.; Krausch, G. Ellipsometric Determination of Flory-Huggins Interaction Parameters in Solution. *Polymer* **2004**, *45*, 7935−7942.
(70) Ogieglo, W.; van der Werf, H.; Tempelman, K.; Wormeester, H.; Wessling, M.; Nijmeijer, A.; Benes, N. E. N-Hexane Induced Swelling of Thin PDMS Films under Non-Equilibrium Nanofiltration Permeation Conditions, Resolved by Spectroscopic Ellipsometry. *J. Membr. Sci.* **2013**, *437*, 313−323.
(71) Papanu, J. S.; Hess, D. W.; Soane, D. S.; Bell, A. T. Dissolution of Thin Poly(methyl Methacrylate) Films in Ketones, Binary Ketone/Alcohol Mixtures, and Hydroxy Ketones. *J. Electrochem. Soc.* **1989**, *136*, 3077−3083.
(72) Papanu, J. S.; Hess, D. W.; Soane (Soong), D. S.; Bell, A. T. Swelling of Poly(methyl Methacrylate) Thin Films in Low Molecular Weight Alcohols. *J. Appl. Polym. Sci.* **1990**, *39*, 803−823.
(73) Sirard, S. M.; Green, P. F.; Johnston, K. P. Spectroscopic Ellipsometry Investigation of the Swelling of Poly(Dimethylsiloxane) Thin Films with High Pressure Carbon Dioxide. *J. Phys. Chem. B* **2001**, *105*, 766−772.
(74) Stamatialis, D. F.; Sanopoulou, M.; Raptis, I. Swelling and Dissolution Behavior of Poly(methyl Methacrylate) Films in Methyl Ethyl Ketone/methyl Alcohol Mixtures Studied by Optical Techniques. *J. Appl. Polym. Sci.* **2002**, *83*, 2823−2834.
(75) Chen, D.; Liu, F.; Wang, C.; Nakahara, A.; Russell, T. P. Bulk Heterojunction Photovoltaic Active Layers via Bilayer Interdiffusion. *Nano Lett.* **2011**, *11*, 2071−2078.

DOI: 10.1021/acs.jpcc.6b03300
J. Phys. Chem. C 2016, 120, 22115−22125

(76) Vohra, V.; Arrighetti, G.; Barba, L.; Higashimine, K.; Porzio, W.; Murata, H. Enhanced Vertical Concentration Gradient in Rubbed P3HT:PCBM Graded Bilayer Solar Cells. *J. Phys. Chem. Lett.* **2012**, *3*, 1820−1823.
(77) Vohra, V.; Higashimine, K.; Murakami, T.; Murata, H. Addition of Regiorandom Poly (3-Hexylthiophene) to Solution Processed Graded Bilayers to Tune the Vertical Concentration Gradient. *Appl. Phys. Lett.* **2012**, *101*, 173301.
(78) Chiu, M.-Y.; Jeng, U.-S.; Su, M.-S.; Wei, K.-H. Morphologies of Self-Organizing Regioregular Conjugated Polymer/Fullerene Aggregates in Thin Film Solar Cells. *Macromolecules* **2010**, *43*, 428−432.
(79) Lou, S. J.; Szarko, J. M.; Xu, T.; Yu, L.; Marks, T. J.; Chen, L. X. Effects of Additives on the Morphology of Solution Phase Aggregates Formed by Active Layer Components of High-Efficiency Organic Solar Cells. *J. Am. Chem. Soc.* **2011**, *133*, 20661−20663.
(80) Tang, H.; Lu, G.; Li, L.; Li, J.; Wang, Y.; Yang, X. Precise Construction of PCBM Aggregates for Polymer Solar Cells via Multi-Step Controlled Solvent Vapor Annealing. *J. Mater. Chem.* **2010**, *20*, 683−688.

DOI: 10.1021/acs.jpcc.6b03300
J. Phys. Chem. C 2016, 120, 22115−22125